

Keep your Eyes on the Lane: Attention-guided Lane Detection

Lucas Tabelini¹, Rodrigo Berriel¹, Thiago M. Paixão²,
Claudine Badue¹, Alberto F. De Souza¹, Thiago Oliveira-Santos¹

¹Universidade Federal do Espírito Santo (UFES) ²Instituto Federal do Espírito Santo (IFES)

tabelini@lcad.inf.ufes.br

Abstract

Modern lane detection methods have achieved remarkable performances in complex real-world scenarios, but many have issues maintaining real-time efficiency, which is important for autonomous vehicles. In this work, we propose LaneATT: an anchor-based deep lane detection model, which, akin to other generic deep object detectors, uses the anchors for the feature pooling step. Since lanes follow a regular pattern and are highly correlated, we hypothesize that in some cases global information may be crucial to infer their positions, especially in conditions such as occlusion, missing lane markers, and others. Thus, we propose a novel anchor-based attention mechanism that aggregates global information. The model was evaluated extensively on of the most widely used datasets in the literature. The results show that our method outperforms the current state-of-the-art methods showing both a higher efficacy and efficiency. Moreover, we perform an ablation study and discuss efficiency trade-off options that are useful in practice.

1. Introduction

Deep learning has been essential for recent advances in numerous areas, especially in autonomous driving [2]. Many of the applications of deep learning in self-driving cars are in their perception systems. To be safe around humans, autonomous vehicles have to be aware of their surroundings, including the position of other vehicles and themselves. In the end, the more predictable a car's movement is, the safer it will be for its passengers and pedestrians. Thus, it is important for autonomous vehicles to have information about each lane's exact position, which is the goal of lane detection systems.

Lane detection models have to overcome various challenges. A model that will be used in a real-world scenario should be robust to several adverse conditions, such as extreme light and weather conditions. Moreover, lane markings can be occluded by other objects (e.g., cars), which is an extremely common case for self-driving cars. Some ap-

proaches, such as polynomial regression models, may also suffer from a data imbalance problem caused by the long-tail effect since cases with more accentuated curves are less common. Besides, the model not only has to be robust but also efficient. In several applications, lane detection should perform in real-time, a requirement that many models struggle to cope with.

As the task is important for the development of self-driving cars, there are numerous works in the literature that tackle this problem. Before the advent of deep learning, several methods employed more traditional computer vision techniques, such as Hough lines [3, 1]. More recently, focus has shifted to deep learning approaches with the advance of convolutional neural networks (CNNs) [12, 16, 10, 17]. Usually, the lane detection problem is formulated as a segmentation task, where, given an input image, the output is a segmentation map with per-pixel predictions [16]. Although recent advances in deep learning have enabled the use of segmentation networks in real-time environments [21], various models struggle to work in real-time. Consequently, the number of backbone options for segmentation-based methods is rather limited. Hence, some recent works have proposed solutions in other directions [12, 22]. Apart from that, many other issues are common in works on lane detection, such as the need for a post-processing step (usually a heuristic), long training times, and a lack of source code, which hinders comparisons and reproducibility.

In this work, a method for lane detection that is both faster and more accurate than most existing state-of-the-art methods is presented. We propose an anchor-based single-stage lane detection model called LaneATT. Its architecture enables the use of a lightweight backbone CNN (e.g., ResNet-34 [8]) while maintaining high accuracy. A novel anchor-based attention mechanism to aggregate global information is also proposed. Extensive experimental results are shown on the , along with a comparison with state-of-the-art methods, a discussion on efficiency trade-offs, and an ablation study of our design choices. To summarize, our main contributions are:

- A lane detection method that is more accurate than existing state-of-the-art real-time methods on a large and complex dataset;
- A model that has faster training and inference times than most other models (reaching 250 FPS and almost an order of magnitude less MACs than the method with the previous highest accuracy);
- A novel anchor-based attention mechanism for lane detection which is potentially useful in other domains where the objects being detected are correlated.

2. Related work

Although the first lane detection approaches rely on classical computer vision, substantial progress on accuracy and efficiency has been achieved with recent deep learning methods. Thus, this literature review focuses on deep lane detectors. We first discuss the dominant approaches, which are those based on segmentation [16, 10, 28, 14] or row-wise classification [9, 19, 26], and, subsequently, review solutions in other directions. Finally, the lack of reproducibility (a common issue in lane detection works) is discussed.

Segmentation-based methods. In this approach, predictions are made on a per-pixel basis, classifying each pixel either as lane or background. With the segmentation map generated, a post-processing step is necessary to decode it into a set of lanes. In SCNN [16], the authors propose a scheme specifically designed for long thin structures and show its effectiveness in lane detection. However, the method is slow (7.5 FPS), which hinders its applicability in real-world cases. Since larger backbones are one of the main culprits for slower speeds, the authors in [10] propose a self attention distillation (SAD) module to aggregate contextual information, which allows the use of a more lightweight backbone, achieving a high-performance while maintaining real-time efficiency. In CurveLanes-NAS [25], the authors propose the use of neural architecture search (NAS) to find a better backbone. Although they achieved state-of-the-art results, their NAS is extremely expensive computationally, requiring 5,000 GPU hours per dataset.

Row-wise classification methods. The row-wise classification approach is a simple way to detect lanes based on a grid division of the input image. For each row, the model predicts the most probable cell to contain a part of a lane marking. Since only one cell is selected on each row, this process is repeated for each possible lane in an image. Similar to segmentation methods, it also requires a post-processing step to construct the set of lanes. The method was first introduced in E2E-LMD [26], achieving state-of-the-art results on two datasets. In [19], the authors show

that it is capable of reaching high speed, although some accuracy is lost. This approach is also used in IntRA-KD [9], where the authors introduce knowledge distillation to the lane detection task.

Other approaches. Other approaches have also been proposed in previous works. For instance, in FastDraw [17] the author proposes a novel learning-based approach to decode the lane structures, which avoids the need for clustering post-processing steps (required in segmentation and row-wise classification methods). Although the proposed method is shown to achieve high speeds, it does not perform better than existing state-of-the-art methods in terms of accuracy. The same effect is shown in PolyLaneNet [22], where an even faster model, based on deep polynomial regression, is proposed. In that approach, the model learns to output a polynomial for each lane. Despite its speed, the model struggles with the imbalanced nature of lane detection datasets, as evidenced by the high bias towards straight lanes in its predictions. In Line-CNN [12], an anchor-based method for lane detection is presented. This model achieves state-of-the-art results on a public dataset and promising results on another that is not publicly available. Despite the real-time efficiency, the model is considerably slower than other approaches. Moreover, the code is not public, which makes the results difficult to reproduce. There are also works addressing other parts of the pipeline of a lane detector. In [11], a post-processing method with a focus on occlusion cases is proposed, achieving results considerably higher than other works, but at the cost of notably low speeds (around 4 FPS). To improve results on night images, Liu et al. [14] propose the use of a GAN to generate night images from day ones to be used for training.

Reproducibility. As noted in [22], many of the cited works do not publish the code to reproduce the results reported [12, 17, 26], or, in some cases, the code is only partially public [10, 9]. This hinders deeper qualitative and quantitative comparisons. For instance, the two most common metrics to measure a model’s efficiency are multiply-accumulate operations (MACs) and frames-per-second (FPS). While the first does not depend on the benchmark platform, it is not always a good proxy for the second, which is the true goal. Therefore, FPS comparisons are also hindered by the lack of source code.

Unlike most of the previously proposed methods that managed to achieve high speeds at the cost of accuracy, we propose a method that is both faster and more accurate than existing state-of-the-art ones. In addition, we publish the full code to reproduce the reported results.

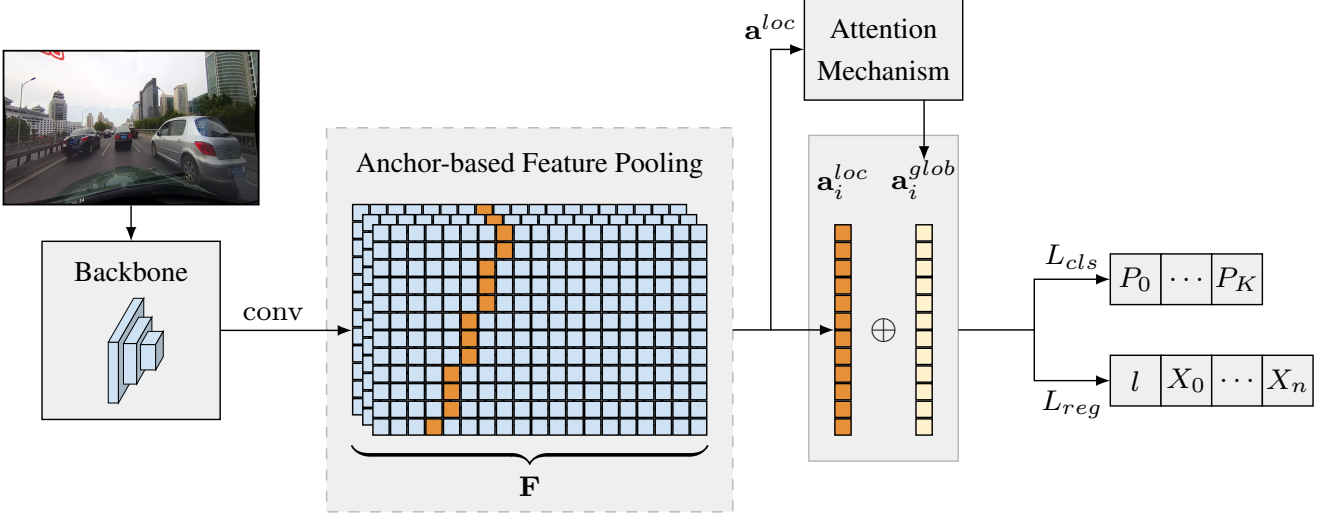


Figure 1: Overview of the proposed method. A backbone generates feature maps from an input image. Then, each anchor is projected onto the feature maps. This projection is used to pool features that are concatenated with another set of features created in the attention module. Finally, using this resulting feature set, two layers, one for classification and another for regression, make the final predictions. The symbol \oplus is used to represent vector concatenation.

3. Proposed method

LaneATT is an anchor-based single-stage model (like YOLOv3 [20] or SSD [15]) for lane detection. An overview of the method is shown in Figure 1. It receives as input RGB images $I \in \mathbb{R}^{3 \times H_I \times W_I}$ taken from a front-facing camera mounted in a vehicle. The outputs are lane boundary lines (hereafter called lanes, following the usual terminology in the literature). To generate those outputs, a convolutional neural network (CNN), referred to as the backbone, generates a feature map that is then pooled to extract each anchor’s features. Those features are combined with a set of global features produced by an attention module. By combining local and global features, the model can use information from other lanes more easily, which might be necessary in cases with conditions such as occlusion or no visible lane markings. Finally, the combined features are passed to fully-connected layers to predict the final output lanes.

3.1. Lane and anchor representation

A lane is represented by 2D-points with equally-spaced y-coordinates $Y = \{y_i\}_{i=0}^{N_{pts}-1}$, where $y_i = i \cdot \frac{H_I}{N_{pts}-1}$. Since Y is fixed, a lane can then be defined only by its x-coordinates $X = \{x_i\}_{i=0}^{N_{pts}-1}$, each x_i associated with the respective $y_i \in Y$. Since most lanes do not cross the whole image vertically, a start-index s and an end-index e are used to define the valid contiguous sequence of X .

Likewise Line-CNN [12], our method performs anchor-based detection using lines instead of boxes, which means that lanes’ proposals are made having these lines as references. An anchor is a “virtual” line in the image plane de-

finied by (i) an origin point (x_{orig}, y_{orig}) (with $y_{orig} \in Y$) located in one of the borders of the image (except the top border) and (ii) a direction θ . The same set of anchors in Line-CNN [12] is used in our method. This lane and anchor representation satisfies the vast majority of real-world lanes.

3.2. Backbone

The first stage of the proposed method is feature extraction, which can be performed by any generic CNN, such as a ResNet [8]. The output of this stage is a feature map $\mathbf{F}_{back} \in \mathbb{R}^{C'_F \times H_F \times W_F}$ from which the features for each anchor will be extracted through a pooling process, as described in the next section. For dimensionality reduction, a 1×1 convolution is applied onto \mathbf{F}_{back} , generating a channel-wise reduced feature map $\mathbf{F} \in \mathbb{R}^{C_F \times H_F \times W_F}$. This reduction is performed to reduce computational costs.

3.3. Anchor-based feature pooling

An anchor defines the points of \mathbf{F} that will be used for the respective proposals. Since the anchors are modeled as lines, the interest points for a given an anchor are those that intercept the anchor’s virtual line (considering the rasterized line reduced to the feature maps dimensions). For every $y_j = 0, 1, 2, \dots, H_F - 1$, there will be a single corresponding x-coordinate

$$x_j = \left\lfloor \frac{1}{\tan \theta} (y_j - y_{orig}/\delta_{back}) + x_{orig}/\delta_{back} \right\rfloor, \quad (1)$$

where (x_{orig}, y_{orig}) and θ are, respectively, the origin point and slope of the anchor’s line, and δ_{back} is the backbone’s

global stride. Thus, every anchor i will have its corresponding feature vector $\mathbf{a}_i^{loc} \in \mathbb{R}^{C_F \cdot H_F}$ (column-vector notation) pooled from \mathbf{F} that carries local feature information (local features). In cases where a part of the anchor is outside the boundaries of \mathbf{F} , \mathbf{a}_i^{loc} is zero-padded.

Notice that the pooling operation is similar to the Fast R-CNN’s [7] region of interest projection (RoI projection), however, instead of using the proposal for pooling, we use the anchor itself given that our method is a single-stage detector. Additionally, the RoI pooling layer (used to generate fixed-size features) is not necessary for our method. Comparing to Line-CNN [12], that leverages only the feature maps’ borders, our method can potentially explore all the feature map, which enables the use of more lightweight backbones with smaller receptive field.

3.4. Attention mechanism

Depending on the model architecture, the information carried by the pooled feature vector ends up being mostly local. This is particularly the case for shallower and faster models, which tend to exploit backbones with smaller receptive fields. However, in some cases (such as the ones with occlusion) the local information may not be enough to predict the lane’s existence and its position. To address that problem, we propose an attention mechanism that acts on the local features (\mathbf{a}_i^{loc}) to produce additional features (\mathbf{a}_i^{glob}) that aggregate global information.

Basically, the attention mechanism structure is composed of a fully-connected layer L_{att} which processes a local feature vector \mathbf{a}_i^{loc} and outputs a probability (weight) $w_{i,j}$ for every anchor j , $j \neq i$. Formally,

$$w_{i,j} = \begin{cases} \text{softmax}(L_{att}(\mathbf{a}_i^{loc}))_j, & \text{if } j < i \\ 0, & j = i \\ \text{softmax}(L_{att}(\mathbf{a}_i^{loc}))_{j-1}, & \text{if } j > i \end{cases} \quad (2)$$

Then, those weights are combined with the local features to produce the global features vector with the same dimensions:

$$\mathbf{a}_i^{glob} = \sum_j w_{i,j} \mathbf{a}_j^{loc}. \quad (3)$$

Naturally, the whole process can be implemented efficiently with matrix multiplication, since the same procedure is executed for all anchors. Let N_{anc} be the number of anchors. Let $\mathbf{A}^{loc} = [\mathbf{a}_1^{loc}, \dots, \mathbf{a}_{N_{anc}}^{loc}]^T$ be the matrix containing the local feature vectors (as rows) and $\mathbf{W} = [w_{i,j}]_{N_{anc} \times N_{anc}}$ the weight matrix, $w_{i,j}$ defined in Equation (2). Thus, global features can be computed as

$$\mathbf{A}^{glob} = \mathbf{W} \mathbf{A}^{loc}. \quad (4)$$

Notice that \mathbf{A}^{glob} and \mathbf{A}^{loc} have the same dimensions, i.e., $\mathbf{A}^{glob} \in \mathbb{R}^{N_{anc} \times C_F \cdot H_F}$.

3.5. Proposal prediction

A lane proposal is predicted for each anchor and consists of three main components: (i) $K + 1$ probabilities (K lane types and one class for “background” or invalid proposal), (ii) N_{pts} offsets (the horizontal distance between the prediction and the anchor’s line), and (iii) the length l of the proposal (the number of valid offsets). The start-index (s) for the proposal is directly determined by the y-coordinate of the anchor’s origin (y_{orig} , see Section 3.1). Thus, the end-index can be determined as $e = s + \lfloor l \rfloor - 1$.

To generate the final proposals, local and global information are aggregated by concatenating \mathbf{a}_i^{loc} and \mathbf{a}_i^{glob} , producing an augmented feature vector $\mathbf{a}_i^{aug} \in \mathbb{R}^{N_{anc} \times 2 \cdot C_F \cdot H_F}$. This augmented vector is fed to two parallel fully-connected layers, one for classification (L_{cls}) and one for regression (L_{reg}), which produce the final proposals. L_{cls} is responsible to predict p_i , i.e., the $K + 1$ probabilities (item i), while L_{reg} outputs r_i , i.e., l and the N_{pts} offsets (items ii and iii).

3.6. Non-maximum Supression (NMS)

As usual in anchor-based deep detection, NMS is paramount to reduce the number of false positives. In the proposed method, this procedure is applied both during training and test phases based on the lane distance metric proposed in [12]. The distance between two lanes $X_a = \{x_i^a\}_{i=1}^{N_{pts}}$ and $X_b = \{x_i^b\}_{i=1}^{N_{pts}}$ is computed based on their common valid indices (or y-coordinates). Let $s' = \max(s_a, s_b)$ and $e' = \min(e_a, e_b)$ define the range of those common indices. Then, the lane distance metric is defined as

$$D(X_a, X_b) = \begin{cases} \frac{1}{e' - s' + 1} \cdot \sum_{i=s'}^{e'} |x_i^a - x_i^b|, & e' \geq s' \\ +\infty, & \text{otherwise.} \end{cases} \quad (5)$$

3.7. Model training

During training, the distance metric in Equation (5) is also used to define the positive and negative anchors. First, the metric is used to measure the distance between every anchor (those not filtered in NMS) and the ground-truth lanes. Then, the anchors with distance (Equation (5)) lower than a threshold τ_p are considered positives, while those with distance greater than τ_n are considered negatives. Anchors (and their associated proposals) with distance in between those thresholds are disregarded. The multi-task loss is defined as

$$\mathcal{L}(\{p_i\}, \{r_i\}) = \lambda \sum_i \mathcal{L}_{cls}(p_i, p_i^*) + \sum_i \mathcal{L}_{reg}(r_i, r_i^*), \quad (6)$$

where p_i, r_i are the classification and regression outputs for the anchor i , while p_i^* and r_i^* are the classification and regression targets for the anchor i . For the regression loss,

Dataset	# of images			Max. # of lanes
	Train	Val.	Test	
TuSimple	3,268	358	2,782	5
CULane	88,880	9,675	34,680	4

Table 1: Overview of the datasets used in this work.

only the length l and the x-coordinates values corresponding to indices common to both the proposal and the ground-truth are used to compute it. The common indices (between s' and e') of the x-coordinates are selected similarly to the lane distance (Equation (5)) but with $e' = e_{gt}$ instead of $e' = \min(e_{prop}, e_{gt})$, where e_{prop} and e_{gt} are the end-indexes for the proposal and its associated ground-truth, respectively. If the end-index predicted in the proposal e_{prop} is used, the training may become unstable by converging to degenerate solutions (e.g., e_{prop} might converge to zero). The functions \mathcal{L}_{cls} and \mathcal{L}_{reg} are the Focal Loss [13] and the Smooth L1, respectively. If the anchor i is considered negative, its corresponding \mathcal{L}_{reg} is equal to 0. The factor λ is used to balance the loss components.

3.8. Anchor filtering for speed efficiency

The full set of anchors comprises a total of 2,782 anchors. This elevated number is one of the main factors limiting the model’s speed. Since a large number of anchors will not be useful during the training (e.g., some anchors may have a starting point above the horizon line of all images in the training dataset), the set’s size can be reduced. To choose which anchors are going to be disregarded in both training and test phases, the method measures the number of times each anchor from the training set is marked as positive (using the same criteria as in the training). Finally, only the top- N_{anc} marked anchors are kept for further processing.

4. Experiments

To evaluate the proposed method, the most widely used datasets in other lane detection works were used: . Before describing the experiments performed, we first describe the efficiency metrics and some of the implementation details that were used in the evaluation. In all experiments, the same default metric parameters set by the dataset and used by the related works are used. Then, the datasets and their metrics are described, along with the results achieved. Finally, experiments on efficiency trade-offs and an ablation study on parts of the proposed method are discussed.

Efficiency metrics. Two efficiency-related metrics are reported: frames-per-second (FPS) and multiply-accumulate operations (MACs). One MAC is approximately two float-

ing operations (FLOPs). The FPS metric is computed using a single image per batch and constant inputs, so the metric is not dependent on I/O operations but only in the model’s efficiency.

Implementation details. Except when explicitly indicated, all input images are resized to $H_I \times W_I = 360 \times 640$ pixels. For all training sessions, the Adam optimizer is used for 15 epochs on CULane and 100 epochs on TuSimple (the large discrepancy is due to the large difference between the datasets’ sizes). For data augmentation, a random affine transformation is performed (with translation, rotation, and scaling) along with random horizontal flips. Most experiments and all FPS measures were computed on a machine with an Intel i9-9900KS and a RTX 2080 Ti. The model parameters $N_{pts} = 72$, $N_{anchors} = 1000$, $\tau_p = 15$ and $\tau_n = 20$ were used. In this work, the datasets used provide no information on the lane type (e.g., dashed or solid). Thus, $K = 1$. For more details and parameter values, the code¹ can be accessed, along with each experiment’s configuration.

4.1. TuSimple

Dataset description. TuSimple [23] is a lane detection containing only highway scenes, a scenario that is usually considered easier than street scenes. Despite that, it is one of the most widely used datasets in lane detection works. All images have a resolution of 1280×720 pixels, with at most 5 lanes. The number of images in each partition (train, validation, and test) is shown in Table 1.

Evaluation metrics. On TuSimple, the three standard metrics are false-positive rate (FPR), false-negative rate (FNR), and accuracy. The accuracy of a single lane on TuSimple is defined as

$$\text{Acc} = \frac{\sum_{clip} C_{clip}}{\sum_{clip} S_{clip}}, \quad (7)$$

where C_{clip} is the number of lane points predicted correctly in the clip and S_{clip} is the total number of points in the clip (or image). For a point prediction to be considered correct, the prediction has to be within 20 pixels the ground truth. For a lane prediction to be considered a true positive (for the FPR and FNR metrics), its accuracy has to be greater than 85%. We also report the F1 score, which is the harmonic mean of the precision and the recall.

Results. The results of LaneATT on TuSimple, along with other state-of-the-art methods, are shown in Table 2 and in Figure 3 (left side). Qualitative results are shown in Figure 2a. As demonstrated, accuracy-wise LaneATT is on

¹

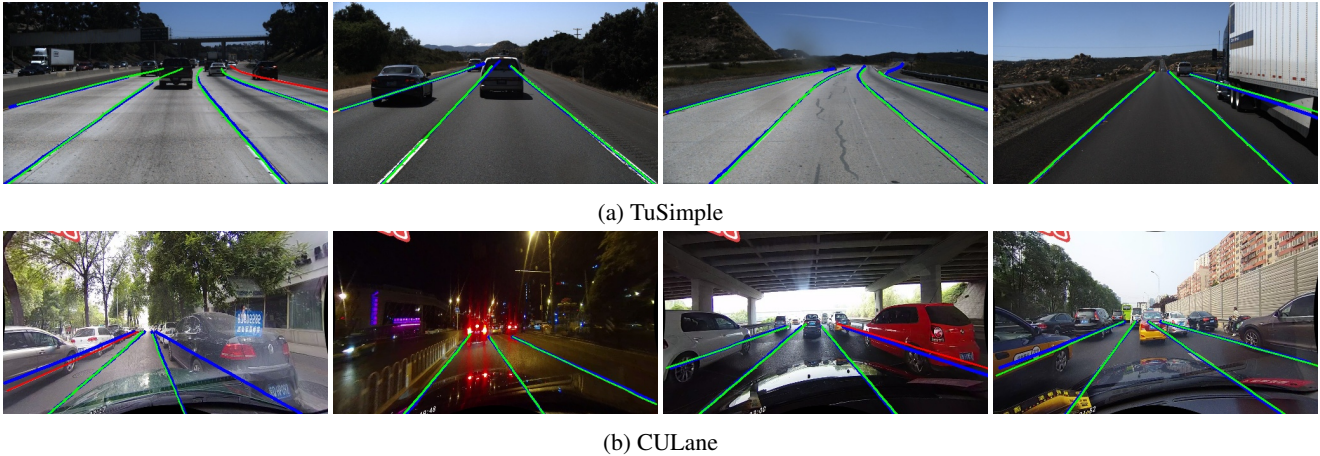


Figure 2: LaneATT qualitative results on TuSimple and CULane. Blue lines are ground-truth, while green and red lines are true-positives and false-positives, respectively.

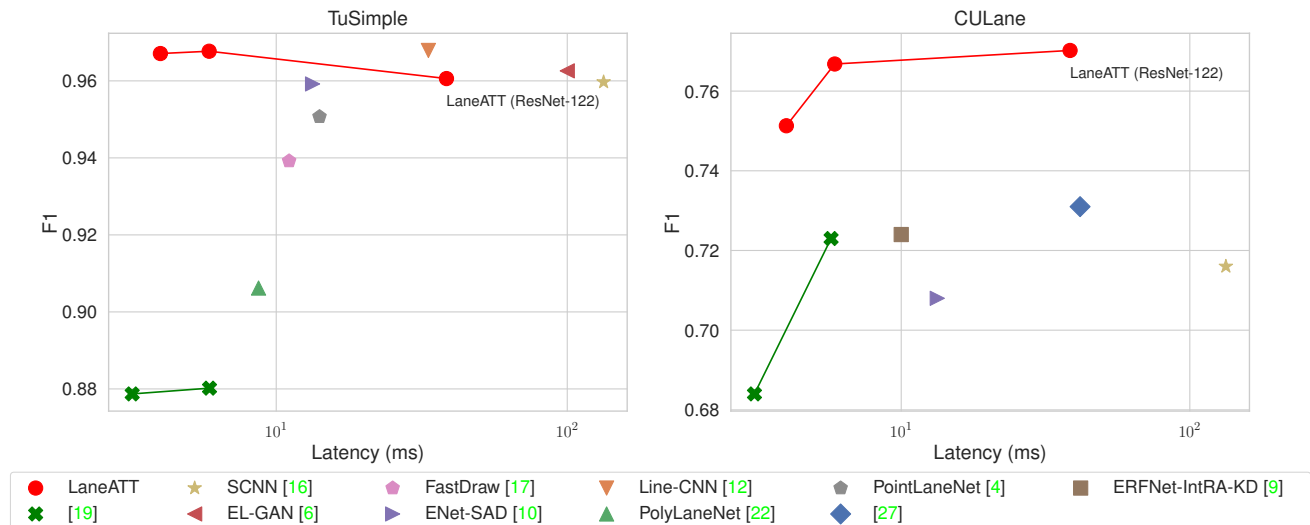


Figure 3: Model latency vs. F1 of state-of-the-art methods on CULane and TuSimple.

par with other state-of-the-art methods. However, it is also clear that the results in this dataset are saturated already, probably because its scenes are not complex and the metric is permissive [22]. This is evidenced by the small difference in performance across methods, in contrast to results in more complex datasets (as shown in Section 4.2). Nonetheless, our method is much faster than others. The only other method that compares to LaneATT with respect to speed is the one proposed in [19]. Since the FPR and FNR metrics were not reported in their work, we computed using the published code and reported those metrics. Although they achieved high accuracy, the FPR is notably high. For instance, our highest false-positive rate is 5.64%, using the ResNet-122 backbone, while their lowest is 18.91%, almost

four times higher.

4.2. CULane

Dataset description. CULane [16] is one of the largest lane detection datasets available publicly, and also one of the most complexes. All images have a resolution of 1640×590 pixels. Moreover, all test images are divided into nine categories, such as crowded, night, absence of visible lines, etc.

Evaluation metrics. The only metric is the F1 score, which is based on the intersection over union (IoU). Since the IoU computation relies on areas instead of points, a

Method	F1 (%)	Acc (%)	FPR (%)	FNR (%)	FPS	MACs (G)
Source-code unavailable						
EL-GAN [6]	96.26	94.90	4.12	3.36	10.0	
Line-CNN [12]	96.79	96.87	4.42	1.97	30.0	
FastDraw (ResNet-18) [17]	94.59	94.90	6.10	4.70		
FastDraw (ResNet-50, adapted) [17]	93.92	95.20	7.60	4.50	90.3	
PointLaneNet [4]	95.07	96.34	4.67	5.18	71.0	
[24]	95.80				71.5	
R-18-E2E [26]	96.40	96.04	3.11	4.09		
R-34-E2E [26]	96.58	96.22	3.08	3.76		
R-50-E2E [26]	96.37	96.11	3.21	4.04		
ERF-E2E [26]	96.25	96.02	3.21	4.28		
Source-code available						
SCNN [16]	95.97	96.53	6.17	1.80	7.5	
Cascaded-CNN [18]	90.82	95.24	11.97	6.20	60.0	
ENet-SAD [10]	95.92	<u>96.64</u>	6.02	<u>2.05</u>	75.0	
[19] (ResNet-18)	87.87	95.82	19.05	3.92	312.5	
[19] (ResNet-34)	88.02	95.86	18.91	3.75	169.5	
PolyLaneNet [22]	90.62	93.36	9.42	9.33	115.0	1.7
LaneATT (ResNet-18)	96.71	95.57	3.56	3.01	<u>250</u>	9.3
LaneATT (ResNet-34)	<u>96.77</u>	95.63	3.53	2.92	171	18.0
LaneATT (ResNet-122)	96.06	96.10	5.64	2.17	26	70.5

Table 2: State-of-the-art results on TuSimple. For a fairer comparison, we measured the FPS of the fastest method ([19]) under the same machine and conditions as our method. Additionally, all metrics for this method were computed using the official source code, since only the accuracy was available in the paper.

lane is represented as a thick line connecting the respective lane’s points. In particular, the dataset’s official metric considers the lanes as 30-pixels-thick lines. If a prediction has an IoU greater than 0.5 with a ground-truth lane, it is considered a true positive.

Results. The results of LaneATT on CULane, along with other state-of-the-art methods, are shown in Table 3 and in Figure 3 (right side). Qualitative results are shown in Figure 2b. We do not compare to the results shown in [11], as the main contribution is a post-processing method that could easily be incorporated to our method, but the source-code is not public. Moreover, this post-processing method makes the model impractical in real world applications, because it is remarkably slow (the full pipeline runs at less than 10 FPS, as reported in their work). In this context, LaneATT achieves the highest F1 among the methods compared while maintaining a high efficiency (+170 FPS) on CULane, a dataset with highly complex scenes. Compared to [19], our most lightweight model (with ResNet-18) surpasses their largest (with ResNet-34) by almost 3% of F1 while being much faster (250 vs. 175 FPS on the same

machine). Additionally, in “Night” and “Shadow” scenes, our method outperforms all other methods, including SIM-CycleGAN [14], a method specifically designed to perform better in those scenarios. Those results demonstrate both the efficacy and the efficiency of LaneATT.

4.3. Efficiency trade-offs

Being efficient is crucial for a lane detection model. In some cases, it might even be necessary to trade some accuracy to achieve the application’s requirement. In this experiment, some of the possible trade-offs are shown. In particular, different settings of image input size ($H_I \times W_I$) and number of anchors ($N_{anchors}$, as described in Section 3.8). The results are shown in Table 4. They show that the number of anchors can be reduced for a slight improvement in terms of efficiency without a large F1 drop. However, if the reduction is too large, the F1 starts to drop considerably. Moreover, if too many anchors are used, the efficacy can also degrade, which might be a consequence of unnecessary anchors disturbing the training. The results are similar for the input size, although the MACs drops are larger. The largest impact of both the number of anchors and the input

Method	Total	Normal	Crowded	Dazzle	Shadow	No line	Arrow	Curve	Cross	Night	FPS	MACs (G)
Source-code unavailable												
[27]	73.10	89.70	76.50	67.40	65.50	35.10	82.20	63.20		68.70	24.0	
FastDraw (ResNet-50) [17]		85.90	63.60	57.00	59.90	40.60	79.40	65.20	7013	57.80	90.3	
PointLaneNet [4]		90.10									71.0	
SpinNet [5]	74.20	90.50	71.70	62.00	72.90	43.20	85.00	50.70		68.10		
SIM-CycleGAN [14]	73.90	91.80	71.80	66.40	76.20	46.10	87.80	67.10	2346	69.40		
R-18-E2E [26]	70.80	90.00	69.70	60.20	62.50	43.20	83.20	70.30	2296	63.30		
R-34-E2E [26]	71.50	90.40	69.90	61.50	68.10	45.00	83.70	69.80	2077	63.20		
R-101-E2E [26]	71.90	90.10	71.20	60.90	68.10	44.90	84.30	70.20	2333	65.20		
ERFNet-E2E [26]	74.00	91.00	73.10	64.50	74.10	46.60	85.80	71.90	2022	67.90		
Source-code available												
SCNN [16]	71.60	90.60	69.70	58.50	66.90	43.40	84.10	64.40	1990	66.10	7.5	
ENet-SAD [10]	70.80	90.10	68.80	60.20	65.90	41.60	84.00	65.70	1998	66.00	75	
[19] (ResNet-18)	68.40	87.70	66.00	58.40	62.80	40.20	81.00	57.90	1743	62.10	322.5	
[19] (ResNet-34)	72.30	90.70	70.20	59.50	69.30	44.40	85.70	69.50	2037	66.70	175.0	
ERFNet-IntRA-KD [9]	72.40										100.0	
CurveLanes-NAS-S [25]	71.40	88.30	68.60	63.20	68.00	47.90	82.50	66.00	2817	66.20		9.0
CurveLanes-NAS-M [25]	73.50	90.20	70.50	65.90	69.30	48.80	85.70	67.50	2359	68.20		33.7
CurveLanes-NAS-L [25]	74.80	90.70	72.30	<u>67.70</u>	70.10	<u>49.40</u>	85.80	68.40	1746	68.90		86.5
LaneATT (ResNet-18)	75.13	91.17	72.71	65.82	68.03	49.13	<u>87.82</u>	63.75	1020	68.58	<u>250</u>	<u>9.3</u>
LaneATT (ResNet-34)	<u>76.68</u>	92.14	75.03	66.47	78.15	49.39	88.38	67.72	1330	<u>70.72</u>	171	18.0
LaneATT (ResNet-122)	77.02	91.74	<u>76.16</u>	69.47	<u>76.31</u>	50.46	86.29	64.05	<u>1264</u>	70.81	26	70.5

Table 3: State-of-the-art results on CULane. Since the images in the ‘‘Cross’’ category have no lanes, the reported number is the amount of false-positives. For a fairer comparison, we measured the FPS of the fastest method ([19]) under the same machine and conditions as our method.

Modification	F1	FPS	MACs	TT (h)
$N_{\text{anchors}} = 250$	68.68	196	17.3	5.7
$N_{\text{anchors}} = 500$	75.45	190	17.4	6.4
$N_{\text{anchors}} = 750$	75.80	181	17.7	7.8
$N_{\text{anchors}} = 1000$	76.66	171	18.0	11.1
$N_{\text{anchors}} = 1250$	75.91	156	18.4	11.5
$H_I \times W_I = 180 \times 320$	66.74	195	4.8	4.3
$H_I \times W_I = 288 \times 512$	75.02	186	11.5	7.3
$H_I \times W_I = 360 \times 640$	76.66	171	18.0	11.1

Table 4: Efficiency trade-offs on CULane using the ResNet-34 backbone. ‘‘TT’’ stands for training time.

size is on the training time. During the inference, the proposals are filtered (using a confidence threshold) before the NMS procedure. During the training, there’s no such filtering. Since the NMS is one the main bottlenecks of the model, and its running time depends directly on the number of objects, the number of anchors has a much higher impact on the training phase than on the testing phase.

4.4. Ablation study

In this experiment the impact of each major part of the proposed method (anchor-based pooling, shared layers, fo-

Model	F1 (%)	FPS	Params. (M)
LaneATT (ResNet-34)	76.68	171	22.13
– anchor-based pooling	64.89	188	21.39
– shared layers	75.45	142	22.34
– focal loss	75.54	171	22.13
– attention mechanism	75.78	196	21.37

Table 5: Ablation study results on CULane.

cal loss and the attention mechanism) is evaluated. The results are shown in Table 5, where the first line contains the result of the standard LaneATT and the next ones of the same model but with a modification. In the second line, the anchor-based pooling was removed and the same procedure to select features of Line-CNN [12] was used (i.e., only features from a single point in the feature map were used for each anchor). In the third one, instead of using a single pair of fully-connected layers (L_R and L_C) for the final prediction, three pairs (six layers) were used, one pair matching one boundary (left, bottom, or right). That is, all anchors starting in the left boundary of the image had its proposals generated by the same pair of layers L_R^L and L_C^L and similarly for the bottom (L_R^B and L_C^B) and the right (L_R^R and L_C^R) boundaries. In the fourth one the Focal Loss was

replaced with the Cross Entropy and in the last one the attention mechanism was removed. The massive drop of performance when the anchor-based pooling procedure is removed shows its importance. This procedure enabled the use of a more lightweight backbone, which was not possible in Line-CNN [12] without a large performance drop. The results also show that a layer for each boundary of the image is not only unnecessary but also detrimental to the model's efficiency. Furthermore, using the Focal Loss instead of the Cross Entropy was also shown to be beneficial. Besides, it also removes the need for one hyperparameter (the number of negative samples to be used in the loss computation). Finally, the proposed attention mechanism is another modification that significantly increases the model performance.

5. Conclusion

We proposed a novel anchor-based single-stage deep lane detection model that outperforms state-of-the-art models, as shown by an extensive comparison with the literature. Not only is the model effective but also efficient. On TuSimple, the method achieves the second-highest reported F1 (a difference of only 0.02%) while being much faster (171 vs. 30 FPS). On CULane, one of the largest and most complex lane detection datasets, the method establishes a new state-of-the-art among real-time methods both in terms of both speed and accuracy (+4.38% of F1 compared to the state-of-the-art method with a similar speed of around 170 FPS). To achieve those results, along with other modifications, a novel anchor-based attention mechanism was also proposed. The ablation study showed that this addition increased the model's performance (F1 score) significantly when considering the gains obtained by the literature advance in the recent years. Additionally, some efficiency trade-offs that are useful in practice were also shown. In future works, this mechanism may be evaluated in other domains where the objects of interest in the scene are correlated.

References

- [1] Abdulhakam AM Assidiq, Othman O Khalifa, Md Rafiqul Islam, and Sheroz Khan. Real time lane detection for autonomous vehicles. In *International Conference on Computer and Communication Engineering*, 2008. 1
- [2] Claudine Badue, R nik Guidolini, Raphael Vivacqua Carneiro, Pedro Azevedo, Vinicius B. Cardoso, Avelino Forechi, Luan Jesus, Rodrigo Berriel, Thiago M. Paix o, Filipe Mutz, Lucas de Paula Veronese, Thiago Oliveira-Santos, and Alberto F. De Souza. Self-driving cars: A survey. *Expert Systems with Applications*, 165:113816, 2021. 1
- [3] Rodrigo F. Berriel, Edilson de Aguiar, Alberto F. De Souza, and Thiago Oliveira-Santos. Ego-Lane Analysis System (ELAS): Dataset and Algorithms. *Image and Vision Computing*, 68:64–75, 2017. 1
- [4] Zhenpeng Chen, Qianfei Liu, and Chenfan Lian. Point-LaneNet: Efficient end-to-end CNNs for Accurate Real-Time Lane Detection. In *Intelligent Vehicles Symposium (IV)*, 2019. 6, 7, 8
- [5] Ruochen Fan, Xuanrun Wang, Qibin Hou, Hanchao Liu, and Tai-Jiang Mu. SpinNet: Spinning Convolutional Network for Lane Boundary Detection. *Computational Visual Media*, 5(4):417–428, 2019. 8
- [6] Mohsen Ghafoorian, Cedric Nugteren, N ra Baka, Olaf Booi, and Michael Hofmann. EL-GAN: Embedding Loss Driven Generative Adversarial Networks for Lane Detection. In *European Conference on Computer Vision (ECCV)*, 2018. 6, 7
- [7] Ross Girshick. Fast R-CNN. In *International Conference on Computer Vision (ICCV)*, 2015. 4
- [8] Kaiming He, Xiangyu Zhang, Shaoqing Ren, and Jian Sun. Deep Residual Learning for Image Recognition. In *Conference on Computer Vision and Pattern Recognition (CVPR)*, 2016. 1, 3
- [9] Yuenan Hou, Zheng Ma, Chunxiao Liu, Tak-Wai Hui, and Chen Change Loy. Inter-Region Affinity Distillation for Road Marking Segmentation. In *Conference on Computer Vision and Pattern Recognition (CVPR)*, 2020. 2, 6, 8
- [10] Yuenan Hou, Zheng Ma, Chunxiao Liu, and Chen Change Loy. Learning lightweight Lane Detection CNNs by Self Attention Distillation. In *International Conference on Computer Vision (ICCV)*, 2019. 1, 2, 6, 7, 8
- [11] Hussam Ullah Khan, Afsheen Rafaqat Ali, Ali Hassan, Ahmed Ali, Wajahat Kazmi, and Aamer Zaheer. Lane Detection using Lane Boundary Marker Network with Road Geometry Constraints. In *Winter Conference on Applications of Computer Vision (WACV)*, 2020. 2, 7
- [12] Xiang Li, Jun Li, Xiaolin Hu, and Jian Yang. Line-CNN: End-to-end traffic line detection with line proposal unit. *Transactions on Intelligent Transportation Systems*, 21:248–258, 2019. 1, 2, 3, 4, 6, 7, 8, 9
- [13] Tsung-Yi Lin, Priya Goyal, Ross Girshick, Kaiming He, and Piotr Doll r. Focal Loss for Dense Object Detection. In *Conference on Computer Vision and Pattern Recognition (CVPR)*, 2017. 5
- [14] Tong Liu, Zhaowei Chen, Yi Yang, Zehao Wu, and Haowei Li. Lane Detection in Low-light Conditions Using an Efficient Data Enhancement: Light Conditions Style Transfer. In *Intelligent Vehicles Symposium (IV)*, 2020. 2, 7, 8
- [15] Wei Liu, Dragomir Anguelov, Dumitru Erhan, Christian Szegedy, Scott Reed, Cheng-Yang Fu, and Alexander C Berg. SSD: Single Shot Multibox Detector. In *European Conference on Computer Vision (ECCV)*. Springer, 2016. 3
- [16] Xingang Pan, Jianping Shi, Ping Luo, Xiaogang Wang, and Xiaoou Tang. Spatial As Deep: Spatial CNN for Traffic Scene Understanding. In *AAAI Conference on Artificial Intelligence (AAAI)*, February 2018. 1, 2, 6, 7, 8
- [17] Jonah Philion. FastDraw: Addressing the Long Tail of Lane Detection by Adapting a Sequential Prediction Network. In *Conference on Computer Vision and Pattern Recognition (CVPR)*, 2019. 1, 2, 6, 7, 8

- [18] Fabio Pizzati, Marco Allodi, Alejandro Barrera, and Fernando García. Lane Detection and Classification using Cascaded CNNs. In *International Conference on Computer Aided Systems Theory*, 2019. 7
- [19] Zequn Qin, Huanyu Wang, and Xi Li. Ultra Fast Structure-aware Deep Lane Detection. In *European Conference on Computer Vision (ECCV)*, 2020. 2, 6, 7, 8
- [20] Joseph Redmon, Santosh Divvala, Ross Girshick, and Ali Farhadi. You Only Look Once: Unified, Real-Time Object Detection. In *Conference on Computer Vision and Pattern Recognition (CVPR)*, 2016. 3
- [21] Eduardo Romera, José M Alvarez, Luis M Bergasa, and Roberto Arroyo. ERFNet: Efficient Residual Factorized ConvNet for Real-Time Semantic Segmentation. *Transactions on Intelligent Transportation Systems*, 19(1):263–272, 2017. 1
- [22] Lucas Tabelini, Rodrigo Berriel, Thiago M. Paixão, Claudine Badue, Alberto F. De Souza, and Thiago Oliveira-Santos. PolyLaneNet: Lane Estimation via Deep Polynomial Regression. In *International Conference on Pattern Recognition (ICPR)*, 2020. 1, 2, 6, 7
- [23] TuSimple. Tusimple benchmark. <https://github.com/TuSimple/tusimple-benchmark>. Accessed September, 2020. 5
- [24] Wouter Van Gansbeke, Bert De Brabandere, Davy Neven, Marc Proesmans, and Luc Van Gool. End-to-end Lane Detection through Differentiable Least-Squares Fitting. *arXiv preprint arXiv:1902.00293*, 2019. 7
- [25] Hang Xu, Shaoju Wang, Xinyue Cai, Wei Zhang, Xiaodan Liang, and Zhenguo Li. CurveLane-NAS: Unifying Lane-Sensitive Architecture Search and Adaptive Point Blending. In *European Conference on Computer Vision (ECCV)*, 2020. 2, 8
- [26] Seungwoo Yoo, Hee Seok Lee, Heesoo Myeong, Sungrack Yun, Hyoungwoo Park, Janghoon Cho, and Duck Hoon Kim. End-to-End Lane Marker Detection via Row-wise Classification. In *Conference on Computer Vision and Pattern Recognition Workshops (CVPRW)*, 2020. 2, 7, 8
- [27] Jie Zhang, Yi Xu, Bingbing Ni, and Zhenyu Duan. Geometric Constrained Joint Lane Segmentation and Lane Boundary Detection. In *the European Conference on Computer Vision (ECCV)*, 2018. 6, 8
- [28] Qin Zou, Hanwen Jiang, Qiyu Dai, Yuanhao Yue, Long Chen, and Qian Wang. Robust Lane Detection from Continuous Driving Scenes using Deep Neural Networks. *Transactions on Vehicular Technology*, 69(1):41–54, 2019. 2